Acta Pharmaceutica Sinica B 2017;7(1):97–105

Chinese Pharmaceutical Association
Institute of Materia Medica, Chinese Academy of Medical Sciences

Acta Pharmaceutica Sinica B

www.elsevier.com/locate/apsb
www.sciencedirect.com

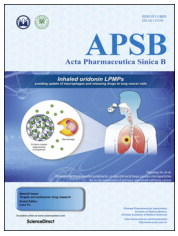

ORIGINAL ARTICLE

Structure of the 40S ribosomal subunit of *Plasmodium falciparum* by homology and *de novo* modeling

Harrison Ndung'u Mwangi[a], Peter Wagacha[b], Peterson Mathenge[b], Fredrick Sijenyi[c], Francis Mulaa[d,*]

[a]*Center for Biotechnology and Bioinformatics, Chiromo Campus, University of Nairobi. HEP Bioinformatics Consultants Ltd., Nairobi, Kenya*
[b]*Department of Computing Informatics, University of Nairobi, Nairobi, Kenya*
[c]*DNA Software, Inc., MI 48104, USA*
[d]*Department of Biochemistry, Riverside Drive, Chiromo Campus, University of Nairobi, Nairobi, Kenya*

Received 27 April 2016; revised 13 June 2016; accepted 5 September 2016

KEY WORDS

Ribosome;
40S subunit;
RNA structure;
Plasmodium falciparum;
3D modeling;
De novo;
Homology

Abstract Generation of three dimensional structures of macromolecules using *in silico* structural modeling technologies such as homology and *de novo* modeling has improved dramatically and increased the speed by which tertiary structures of organisms can be generated. This is especially the case if a homologous crystal structure is already available. High-resolution structures can be rapidly created using only their sequence information as input, a process that has the potential to increase the speed of scientific discovery. In this study, homology modeling and structure prediction tools such as RNA123 and SWISS–MODEL were used to generate the 40S ribosomal subunit from *Plasmodium falciparum.* This structure was modeled using the published crystal structure from *Tetrahymena thermophila*, a homologous eukaryote. In the absence of the *Plasmodium falciparum* 40S ribosomal crystal structure, the model accurately depicts a global topology, secondary and tertiary connections, and gives an overall root mean square deviation (RMSD) value of 3.9 Å relative to the template's crystal structure. Deviations are somewhat larger in areas with no homology between the templates. These results demonstrate that this approach has the power to identify motifs of interest in RNA and identify potential drug targets for macromolecules whose crystal structures are unknown. The results also show the utility of RNA homology modeling software for structure determination and lay the groundwork for applying this

*Corresponding author. Fax: +254 0204442841.
E-mail address: mulaafj@uonbi.ac.ke (Francis Mulaa).

Peer review under responsibility of Institute of Materia Medica, Chinese Academy of Medical Sciences and Chinese Pharmaceutical Association.

http://dx.doi.org/10.1016/j.apsb.2016.10.003

approach to larger and more complex eukaryotic ribosomes and other RNA-protein complexes. Structures generated from this study can be used in *in silico* screening experiments and lead to the determination of structures for targets/hit complexes.

1. Introduction

Knowledge of the structure of pathogen ribosomes[1,2] is important for the development of new narrow-spectrum (species-selective) and broad-spectrum antibiotics. According to the Centers for Disease Control and Prevention (CDC), the majority of hospital-acquired infections involves drug-resistant pathogens[3]. Of particular concern are drug-resistant *Plasmodium falciparum, Mycobacterium tuberculosis, Pseudomonas aeruginosa, Enterococcus, Escherichia coli and Staphylococcus aureus*. Development of new drugs against *P. falciparum and M. tuberculosis* is particularly important in view of the high risk of drug resistance they pose[3,4]. A major step towards better drug design is understanding the biological structure of the target which, for many antibiotics is the ribosome[5]. Thus, drug development can be expedited if the ribosomal structures for these different organisms are known.

In the last decade, a number of ribosome crystal structures have been determined[5–8]. However, despite great effort, the only organisms for which ribosome structures have been determined with atomic resolution are the thermophilic bacterium *Thermus thermophilus* (high resolution of the 30S, and low resolution of the 70S), the archeaon *Haloarcula marismortui* (high resolution of 50S only), and the eubacterium *Deinococcus radiodurans* (high resolution of 50S only)[9–11]. Thus, there is a need to predict the ribosome structures of other pathogenic prokaryotes and eukaryotes. Recently, software has been developed that can use known ribosome structures to model the structures of ribosomes from homologous organisms. Such software is capable of accounting for substitutions, deletions and insertions as well as chemical modifications in the ribosomes of other organisms[12,13]. The methods described in this paper provide tools for modeling complex nucleic acid molecules using known structures of homologous nucleic acids from other organisms. These methods will also show that *de novo* techniques can be used to model complex nucleic acids by referencing databases of known structural motifs.

By using advanced structural techniques, such as electron microscopy and nuclear magnetic resonance, new information can be generated to help understand the eukaryotic ribosome. However, generation of high resolution X-ray structures of eukaryotic 80S ribosomes lags behind that of bacteria due to their greater complexity[14,15]. Cyro-electron microscopy and single particle reconstruction have been used to determine structures of a transplanting plant 80S ribosome at 5.5 Å resolution which maps together with the 6.1 Å resolution of the *Saccharomyces cerevisiae* 80S ribosome[16]. Furthermore, recent advances in crystallographic methods[7] has led to the determination of the first X-ray structure of the yeast ribosome at 3.0 Å resolution[6]. Importantly, this has facilitated ribosomal comparisons of different species and kingdoms of life and should assist in understanding the biochemical interaction between the eukaryotic ribosome and molecules in basic life forms. Eukaryotic ribosomes are more complex than their prokaryotic counterparts and synthesis of their proteins differs at the level of initiation although their core functions are conserved[17]. Determining the structure of the *P. falciparum* 40S ribosome will lead to a better understanding of the structural basis for protein synthesis in the cell. It will also enable researchers to run *in silico* ligand screening experiments of potential anti-malarial compounds.

The eukaryotic ribosome contains two subunits, the small 40S subunit comprised of 18S rRNA and 33 proteins and the large 60S subunit composed of the 28S, 5S, 5.8S and 49 proteins[6,7,18]. The eukaryotic ribosome is highly complex with a molecular mass of ~4 million Da compared to 2.8 million Da for the prokaryote ribosome[19–21]. The small 40S subunit is larger by almost 500 kDa than the prokaryotic small 30S subunit[5,22,23]. In the 40S subunit, the 18S rRNA has three notable sequence insertions known as expansion segments (ES). ES3 is located in the 5′ major domain, ES6 and ES7 in the central domain, ES9 in the 3′ major domain and ES12 in the 3′ minor domain[24]. The eukaryotic 40S subunit contains ~30 proteins, 18 of which do not have homologs in bacteria and its 18S rRNA comprises about 45% of its mass[20,25]. Recent publications of eukaryotic 40S ribosome structures, such as that of *Tetrahymena thermophila*[26] show more defined interactions between the ribosomal RNA and proteins.

Homology modeling for evolutionally-related proteins involves two proteins that have a close common ancestor. An alignment score can be obtained to show similarities between the protein sequences, a lower score suggesting different structural and functional moieties[26]. Inaccuracies in homology models are often traced to lower sequence identity between the two proteins[27]. RNA modeling is more challenging than protein modeling due to structural complexities associated with RNA. For instance, the RNA backbone has 6 dihedral angles while proteins have only two. In addition, RNA residues are substantially larger in size than protein residues. Various research groups have attempted to increase the size limit and accuracy of predicted RNA structures by developing appropriate software. A good example is RNA123 which is a suite of tools for homology modeling, *de novo* structure prediction and analysis of RNA structures[12]. The modeling processes a series of algorithms to account for substitutions, insertions, deletion and gap closing, and performs a final energy minimization to obtain a low energy structure.

2. Methods

Most homology modeling involves four steps, *viz* template selection, target template alignment, model building and evaluation of the model. Modeling of a structure is achieved by interactively repeating these steps until the desired model is produced. A number of different techniques for model building have been developed to meet the growing demand for accurate structures[28–30]. The approach

adopted by the SWISS-MODEL server can best be described as rigid fragment assembly which was first implemented in RNA Composer[30]. In this study, template-based modeling was used in conjunction with *de novo* prediction of motifs that were lacking in the template but present in the sequence.

2.1. *Proof of concept*

To provide proof of concept, we used homology modeling to generate structures of the 40S subunit of *S. cerevisiae* (RSCB ID 4V7R) from the crystal structure of the homologous eukaryotic 40S ribosomal subunit of *T. thermophila* (RSCB ID 4V5O). Sequence information homology modeling methodology was followed to obtain the model structure. The models generated were then superimposed on the actual crystal structure and the root mean square deviation (RMSD) calculated. Based on the results, we concluded the homology modeling technique was useful to rapidly generate reliable structures but it depended on the similarity of the two organisms. We also concluded that it could expedite generation of structures of organisms for which no structures were available (Table 1).

Table 1 Root mean square deviation results for the modeled *Tetrahymena thermophila* domains superimposed on the X-ray crystallographic structure of *T. thermophila* and on the template of *Saccharomyces cerevisiae*.

Modeled domain	RMSD (Å)	
	T. thermophila (4V5O)	*S. cerevisiae* (4V7R)
3′ Minor	1.94	3.98
3′ Major	2.68	4.24
Central	3.94	3.67
5′ Major	1.28	3.62

In this study, we employed the software for RNA homology modeling developed by Dr. John Santa Lucia of Wayne University that allows prediction of mutant structures given the X-ray structure of a reference sequence. The accuracy of the predictions was validated for several rRNA domains with sequence identity as low as 50%, and predicted structures with all-atom RMSD close to 2 Å were typically obtained[12]. For the whole *P. falciparum* structure, much higher levels of sequence identity were obtained and thus the homology predictions reported in this study are highly accurate.

2.2. *Template selection*

For the 18S rRNA modeling of *P. falciparum*, we selected a homologous crystal structure (PDB ID 4V5O) to be used as the template. For the 40S ribosomal proteins, the template was selected based on a homology score after sequence alignment.

2.3. *Alignment*

18S rRNA sequence alignment was achieved by first dividing the entire 18S rRNA into its constituent domains (Fig. 1, 3′ minor, 3′ major, central and 5′ major domains). Since domains fold independently, this approach was chosen as it simplifies the examination and correction of the resultant alignments. For the 40S proteins, generation of the structure alignment was done in SWISS MODEL where a local pairwise alignment of the target sequence to the main template structures was calculated followed by a heuristic step to improve the alignment for modeling purposes. The placement of insertions and deletions was optimized considering the template structure context.

2.4. *Model building*

Generation of the model core was initiated by averaging the backbone atom positions of the *T. thermophila* template structure. This was followed by assessing sequence similarity by target

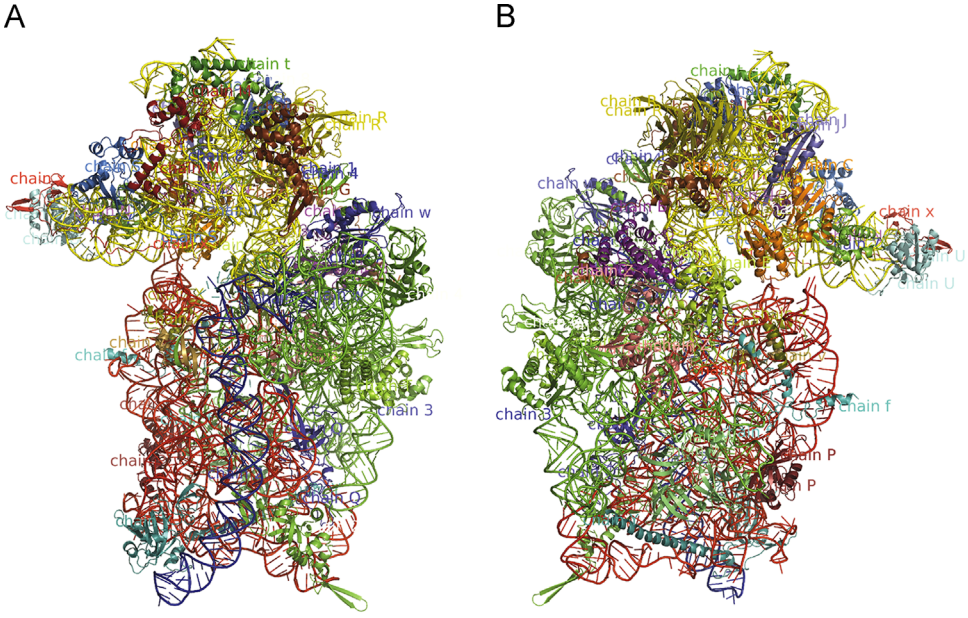

Figure 1 Tertiary structure of *Plasmodium falciparum* 40S front (A) and back view (B). Domains are colored (5′ major: red; central: yellow; 3′ major: blue and 3′ minor: green). Also shown are the 34 40S ribosomal proteins of *Plasmodium falciparum* interacting with the 18S rRNA to make the total subunit.

(*P. falciparum*)-template (*T. thermophila*) alignment. To do this, an assembly of fragments compatible with the neighboring stems was constructed using constraint space programming (CSP) for proteins. In RNA 123, a flow chart of the model building algorithm based on using a fragment library of possible motifs collected from previous crystal structurers is shown in Fig. 2. The algorithm follows a scoring scheme where the best loop/motif is selected based on favorable force field energy, steric hindrance and favorable interactions like hydrogen bond formation. If a suitable loop cannot be identified, the *de novo* algorithm is activated to build the fragments using sequence information alone.

2.5. *Energy minimization*

Deviations in the geometry of the protein or RNA structure introduced by the modeling algorithm when joining rigid fragments are regularized in the last modeling step by steepest descent energy minimization using the GROMOS96 force field[31] in SWISS–MODEL. For RNA123, empirical force fields were used to detect parts of the model with conformational errors. Energy minimization was then performed to correct these errors.

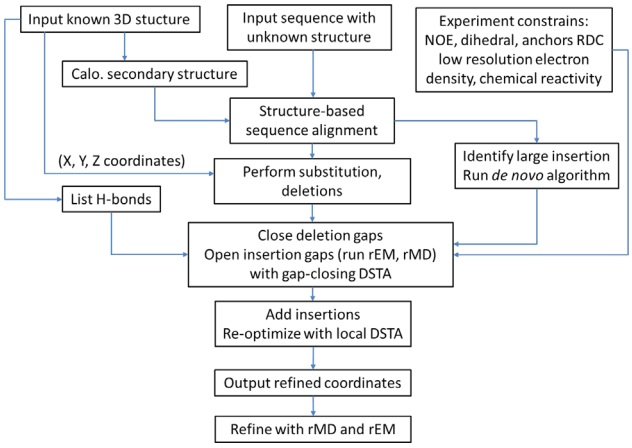

Figure 2 The overall process for performing homology modeling of the *P. falciparum* 40S ribosome as per RNA123.

2.6. *Structure validation*

Validation of models was carried out using several validation tools such as MOL-PROBITY[32], PRO-CHECK and MATCH CHECK[33]. The validation tools help by adding hydrogen atoms to the crystal structure (Supplementary Information).

3. Results and discussion

The first step is to input the coordinates of the known template structure (*i.e.*, the *T. thermophila* 40S structure) and the sequence of the pathogen or other organism (*i.e.*, *P. falciparum*). The second step is to perform a sequence alignment that includes secondary structure constraints. The third step is to use the sequence alignment to guide the substitutions, deletions and insertions to be automatically made in the 3D software. The final step is to optimize the geometry of the structure using molecular dynamics and energy minimization. The ribosomal proteins were also modeled by similar methods using public and commercial servers, such as the Expasy server. This approach was found to be reasonably reliable since *P. falciparum* proteins within the *P. falciparum* domain often have sequence identity $>50\%$.

Due to the complexity of 18S rRNA, its structure was modeled by segmenting it into different domains (5′ major (Fig. 3A), central (Fig. 3B), 3′ major (Fig. 3C) and 3′ minor (Fig. 3D)) and subsequently combining them to form the complete structure (Fig. 3E). Since these domains were generated separately, residue clashes were expected upon combining them. This then requires

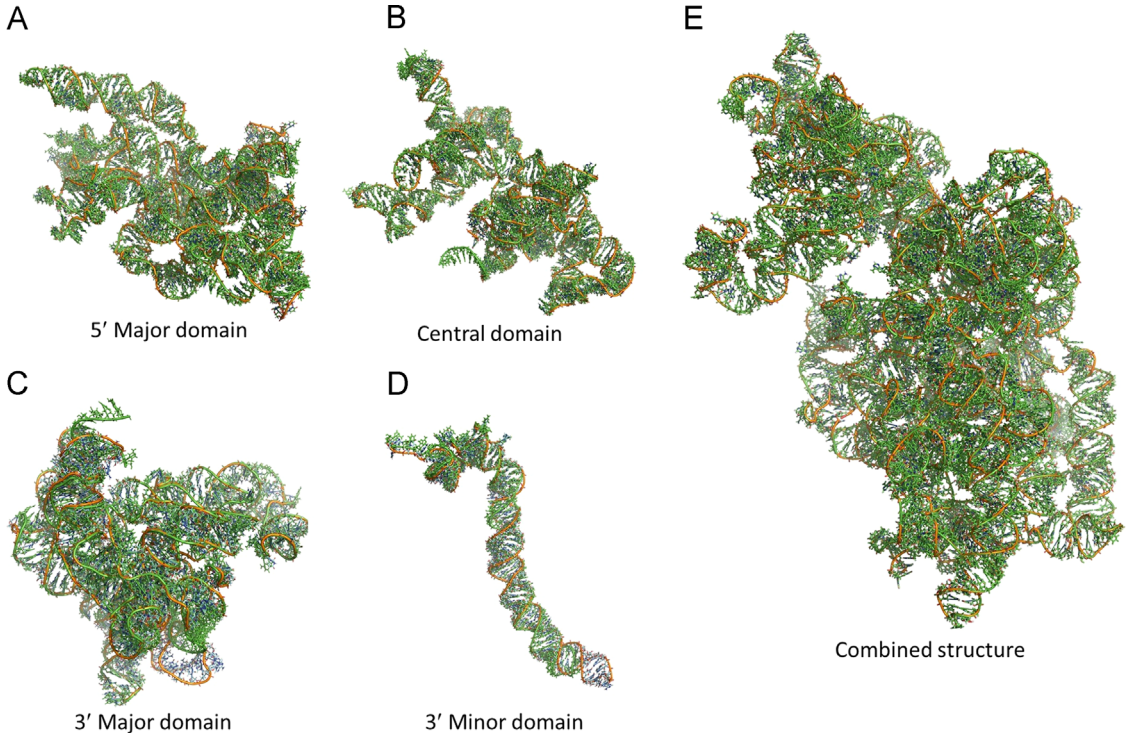

Figure 3 Due to the complexity of 18S rRNA, its structure was modeled by segmenting it into different domains (A) 5′ major domain, (B) central domain, (C) 3′ major domain, and (D) 3′ minor domain, and subsequently combining them to form (E) the complete structure.

Table 2 *Plasmodium falciparum* 18S rRNA energy optimization obtained using RNA123 which helps minimize the energy from a large positive figure to a more acceptable negative figure that is biologically functional.

Name	18S rRNA.std.egy	18S rRNA.opt.egy
Total inter energy	2,410,217.54112	−34,562.06042
Total intra energy (–Gamma En)	−16,765.12946	−16,733.20508
Total gamma terms energy	1,433.94236	1,473.80569
Total gap geometry penalty	2,893.75332	3,454.89615
Total restraint energy	0.00000	6,083.08080
Total structure energy	2,397,780.10735	−46,366.56367

the structure to be subjected to an additional series of energy minimizations (Table 2) in RNA123 to obtain the three dimensional (3D) structure. This was further used to anchor the 34 ribosomal proteins to give the 3D structure of *P. falciparum* (Fig. 4).

18S rRNA is a large biological molecule that performs multiple roles in the coding, unraveling, regulation, and expression of genes and in their translation in eukaryotes. The rRNA has a catalytic role in the ribosome that is orchestrated in the nucleolus.

The longest expansion fragment (ES) in the 18S rRNA of *P. falciparum*, ES6 (Fig. 5), comprises 215 nucleotides framing one helix that replaces the five helices of *T. thermophila* and h21 in bacteria. The single helix that replaces helices A, B, C and D of *T. thermophila* occupies a large part of the back of the 40S body and varies significantly in structure from past models. For example, the helices extend over the back of 40S and are covered by helix A. In addition, the loop region of helix ES6E in *T. thermophila* forms a base pair with ES3B, yielding a broad

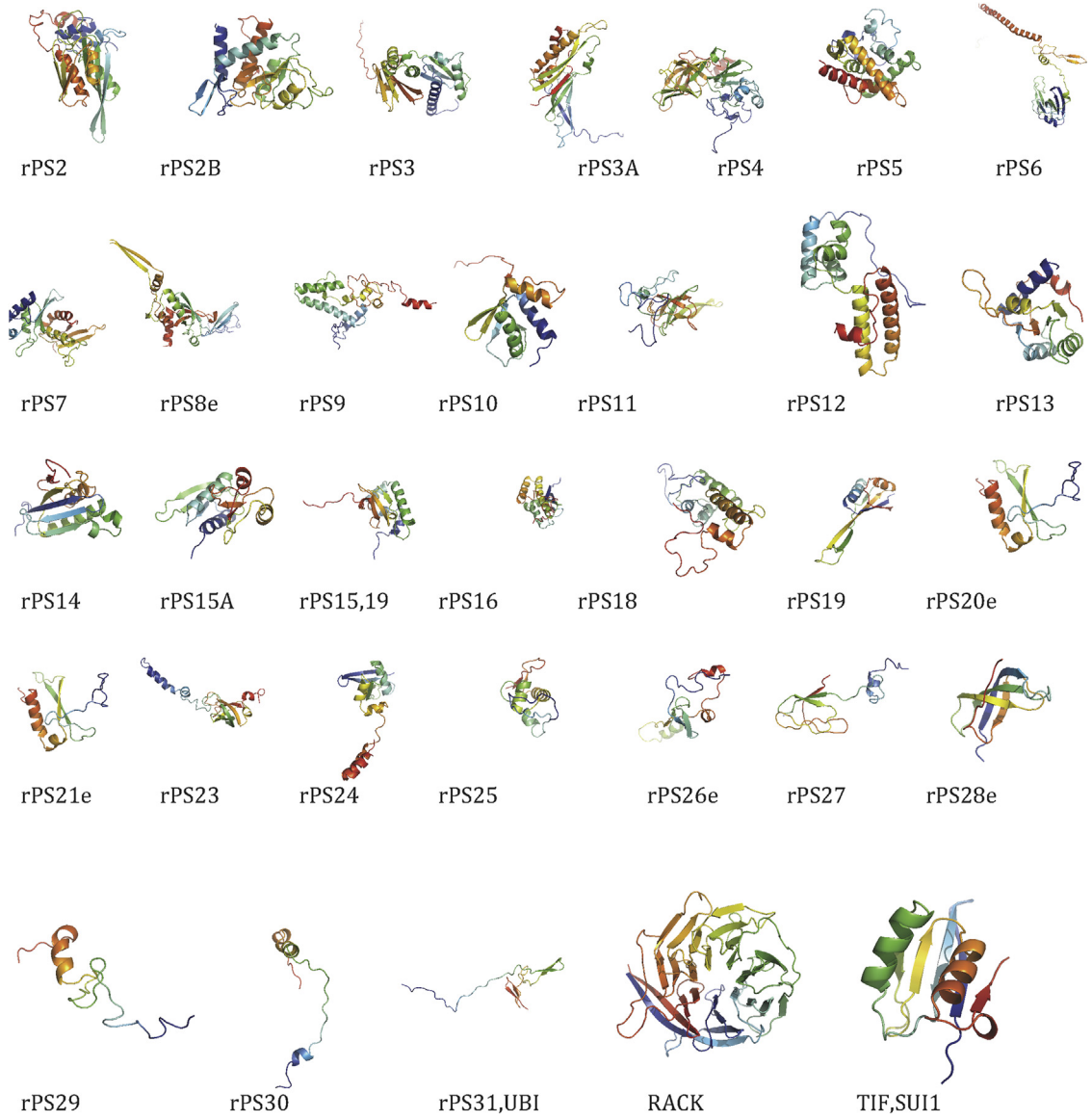

Figure 4 3D structures of all ribosomal proteins of the 40S subunit of *P. falciparum*. The backbone of all proteins is shown in color.

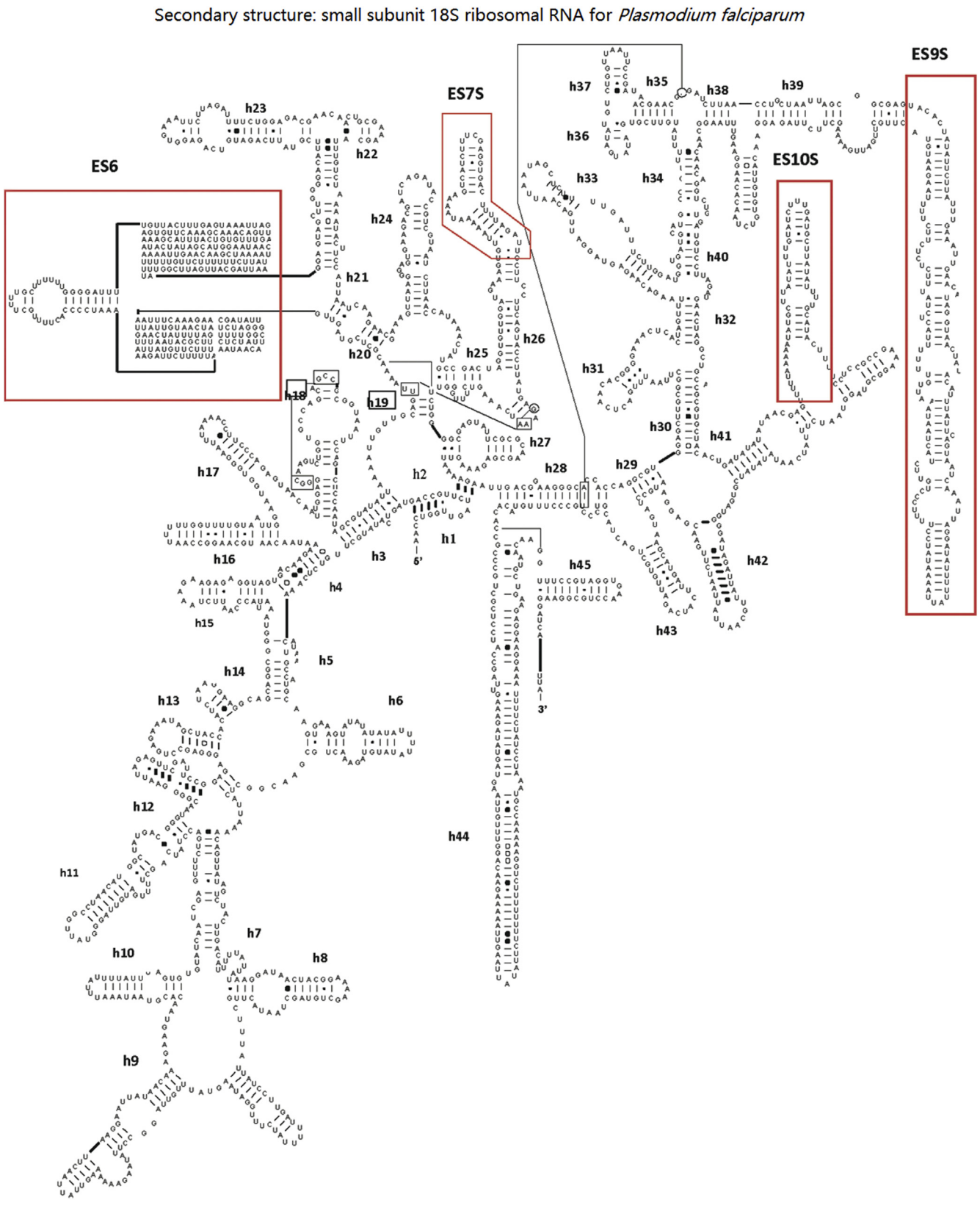

Figure 5 The two-dimensional structure of *P. falciparum* showing the various expansion segments and the various domains.

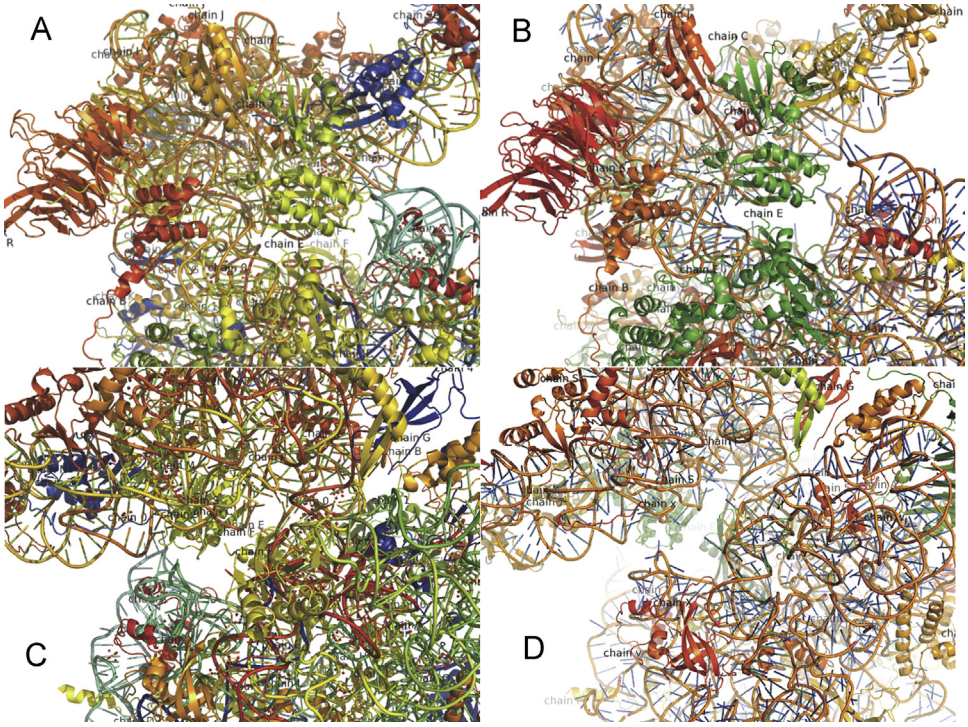

Figure 6 Side by side view of the front and back orientations of *Tetrahymena thermophila* and *Plasmodium falciparum* mRNA tunnels: the front (A) and back (C) views of *T. thermophila,* the front (B) and back (D) views of *P. falciparum*. Ribosomal proteins residue which extends into the mRNA channel site at the ribosomal head and shoulder can be easily recognized.

helix that ventures from the focal point of the back towards the left foot of 40S[20,34,35]. The quaternary interaction of ES3 and ES6, together with several proteins, frames another area of the more extensive back and more conspicuous left foot elements of 40S as in *T. thermophila*.

The homologous structure of the 40S subunit of *P. falciparum* provides insights into the evolution of the parasite ribosome and its specific functions. It also reveals the interactions of the ribosomal RNA and proteins providing a step towards understanding eukaryotic parasite translation. We anticipate it may provide a new direction in targeting the small differences in host-parasite translation to bring about a major decline in parasitic illnesses.

During secondary structure alignment by RNA123, specific deletions or insertions that account for genus specific differences appear as gaps or insertions. They occur mostly in central regions at h16–h17, ES6, h26–ES7S, ES9S, and ES10S, rather than in the highly conserved 5′ and 3′ ends (Fig. 5). It is encouraging to note that the secondary structure of two different organisms can appear very similar despite the fact that their molecular length is totally different. After secondary structure alignment, a consensus sequence can be added to aid the model to conform to its final biological function.

During translation in the ribosome, steric hindrance by elements of mRNA secondary structure is dependent on the activity of the intrinsic helicase that unwinds the mRNA. *P. falciparum* homologs to bacterial rpS3p interact with the mRNA channel, whereas homologs to bacterial rpS4p, *i.e.*, rpS9e, are shorter and do not extend into the mRNA channel[20]. However, the *P. falciparum*–specific rpS30e has three essential residues oriented toward the mRNA channel as in *T. thermophila* and appears to serve as a partial positional and practical analog of bacterial rpS4p[20,36].

The interpretation of bacterial structure begins with the interconnection of two segments of the small ribosomal subunit with the 5′ untranslated section of mRNA. The purpose of the association is the anti–Shine-Dalgarno grouping close to the 3′ end of the 16S rRNA and the ribosomal protein rpS1p in most bacteria[7,13,37]. A homolog of rpS1p or a Shine-Dalgarno grouping is not required to initiate interpretation of either *T. thermophila or P. falciparum*[8,38]. The area corresponding to the bacterial Shine-Dalgarno chamber in the structure of the 40S subunit (where rpS1p has been pictured in electron microscopy investigations of the 30S subunit[25]) is partly occupied by the proteins rpS28e and rpS26e of *P. falciparum* as in *T. thermophile*[20] (Fig. 6). The structure of the RNA binding domain of rpS1p correlates to the b-barrel structure of rpS28e of *P. falciparum*[39–41]. The 3′ end of *P. falciparum* 18S rRNA, in contrast to the flexible 3′ end of bacterial 16S rRNA, appears to be kept in place by rigid connections with rpS26e. Regulation of signaling pathways by rpS4e, rpS6e, and RACK1 is comparable with those in *T. thermophila*[13,16,20].

The crystal structure of the 40S subunit allows an insight into its signaling process. Focus is particularly centered on rpS6e, a target of the mTOR pathway; rpS4e, that is distinctly phosphorylated in both *T. thermophile and P. falciparum* and RACK1, a signaling focal point in the ribosome[13,20]. The *P. falciparum* ribosomal protein, rpS6e, extends from the right to the left foot of the 40S subunit (Fig. 1). Location of the ribosomal protein, rpS4e, is found at the back of the ribosome and is firmly anchored within ES3 and ES6, of 18S rRNA. Both the *P. falciparum* and *T. thermophila* 40S subunits have structures that contain bound RACK1[20,42]. RACK1 makes extensive contacts not only with the phosphate backbone and bases of 18S rRNA, but also with the

ribosomal proteins, rpS16e, rpS17e and rpS3e, all of which modify the signaling properties of RACK1. Undeniably, two eukaryotic signaling protein binding sites in RACK1, the site of phosphorylation, and the binding site of focal adhesion kinase (FAK)[43,44], are at least partially occluded when RACK1 is bound to the ribosome. This may partially explain the result of a recent study in yeast which suggested a correlation between the location of RACK1 at the ribosome and its signaling function[20,43,44].

4. Conclusions

Modeling the structure of the *P. falciparum* 40S ribosomal subunit will lead to a better understanding of the structural basis for its protein-synthesizing role in the cell. The modeling platform allows for generation of a 3D atomic-level structure of pathogenic ribosomes through a combination of homology and *de novo* modeling. The developed RNA platform allows for a systematic study of RNA-ligand interactions and will facilitate the design of drug-like compounds that target biologically functional motifs. Furthermore, it will enable researchers in drug development to run *in silico* ligand screening experiments of a library of potentially active antimalarial compounds against the solved *P. falciparum* 40S structure as a target. Drug leads identified through this method could then lead to further biochemical and *in vitro* binding studies with the ultimate goal of developing new classes of antimalarial drugs. It is anticipated that the structure prediction and modeling technologies used here will dramatically reduce the time it takes from target identification to drug lead determination.

Acknowledgments

We thank Dr. Fred Sijenyi for initial contributions to this project and DNA SOFTWARE Inc. for access to RNA123. This work was supported by European Union Grant Contract No. 018834; Development of New Drugs for the Treatment of Malaria "ANTIMAL, ISP–KEN-02 PROJECT: Drug Discovery from Kenya's Biodiversity and the Chinese Government for travel fellowships to the Institute of Materia Medica Symposium on Drug Discovery of Infectious Diseases, May 2015. Part of this research was conducted at the School of Computing and Informatics, University of Nairobi.

Appendix A. Supplementary material

Supplementary data associated with this article can be found in the online version at http://dx.doi.org/10.1016/j.apsb.2016.10.003.

References

1. Lewis K. Platforms for antibiotic discovery. *Nat Rev Drug Discov* 2013;**12**:371–87.
2. Steitz T, Moore P, Ban N, Nissen P, Hansen J, Inventors. *Ribosome structure and protein synthesis inhibitors*. US Patent 8912150. 2014 Dec 16.
3. Greenwood D, Slack RC, Barer MR, Irving WL. *Medical microbiology: a guide to microbial infections: pathogenesis, immunity, laboratory diagnosis and control*. Amsterdam: Elsevier Health Sciences; 2012.
4. Laxminarayan R, Duse A, Wattal C, Zaidi AK, Wertheim HF, Sumpradit N, et al. Antibiotic resistance—the need for global solutions. *Lancet Infect Dis* 2013;**13**:1057–98.
5. Clemons Jr WM, May JL, Wimberly BT, McCutcheon JP, Capel MS, Ramakrishnan V. Structure of a bacterial 30s ribosomal subunit at 5.5 a resolution. *Nature* 1999;**400**:833–40.
6. Jenner L, Melnikov S, de Loubresse NG, Ben-Shem A, Iskakova M, Urzhumtsev A, et al. Crystal structure of the 80s yeast ribosome. *Curr Opin Struct Biol* 2012;**22**:759–67.
7. Ben-Shem A, Garreau de Loubresse N, Melnikov S, Jenner L, Yusupova G, Yusupov M. The structure of the eukaryotic ribosome at 3.0 Å resolution. *Science* 2011;**334**:1524–9.
8. Yusupova G, Yusupov M. Ribosome biochemistry in crystal structure determination. *RNA* 2015;**21**:771–3.
9. Poehlsgaard J, Douthwaite S. The bacterial ribosome as a target for antibiotics. *Nat Rev Microbiol* 2005;**3**:870–81.
10. Oren A. Characterization of the halophilic archaeal community in saltern crystallizer ponds by means of polar lipid analysis. *Int J Salt Lake Res* 1994;**3**:15–29.
11. Baumeister W, Barth M, Hegerl R, Guckenberger R, Hahn M, Saxton W. Three-dimensional structure of the regular surface layer (HPI layer) of *Deinococcus radiodurans*. *J Mol Biol* 1986;**187**:241–50.
12. Sijenyi F, Saro P, Ouyang Z, Damm-Ganamet K, Wood M, Jiang J, et al. The RNA folding problems: different levels of srna structure prediction. In: Leontis N, Westhof, editors. *RNA 3D structure analysis and prediction*. Berlin Heidelberg: Springer; 2012. p. 91–117.
13. Mwangi HN. Structure of the 40S ribosomal subunit from *Plasmodium falciparum* by homology and *de novo* modeling [dissertation]. Nairobi: University of Nairobi; 2013.
14. Dinman JD. The eukaryotic ribosome: current status and challenges. *J Biol Chem* 2009;**284**:11761–5.
15. McLennan A, Bates A, Turner P, White M. *Bios instant notes in molecular biology*. 4th ed. London: Taylor & Francis; 2012.
16. Wilson DN, Doudna Cate JH. The structure and function of the eukaryotic ribosome. *Cold Spring Harb Perspect Biol* 2012;**4**:pii:a011536.
17. Jenner LB, Ben-Shem A, Demeshkina N, Yusupov M, Yusupova G. X-ray analysis of prokaryotic and eukaryotic ribosomes. In: Dinman JD, editor. *Biophysical approaches to translational control of gene expression*. New York: Springer; 2013. p. 1–25.
18. Carter AP, Clemons WM, Brodersen DE, Morgan-Warren RJ, Wimberly BT, Ramakrishnan V. Functional insights from the structure of the 30S ribosomal subunit and its interactions with antibiotics. *Nature* 2000;**407**:340–8.
19. Ben-Shem A, Jenner L, Yusupova G, Yusupov M. Crystal structure of the eukaryotic ribosome. *Science* 2010;**330**:1203–9.
20. Rabl J, Leibundgut M, Ataide SF, Haag A, Ban N. Crystal structure of the eukaryotic 40S ribosomal subunit in complex with initiation factor 1. *Science* 2011;**331**:730–6.
21. Bielka H. *The eukaryotic ribosome*. Berlin: Springer; 338.
22. Taylor DJ, Devkota B, Huang AD, Topf M, Narayanan E, Sali A, et al. Comprehensive molecular structure of the eukaryotic ribosome. *Structure* 2009;**17**:1591–604.
23. Dresios J, Panopoulos P, Synetos D. Eukaryotic ribosomal proteins lacking a eubacterial counterpart: important players in ribosomal function. *Mol Microbiol* 2006;**59**:1651–63.
24. Hashem Y, des Georges A, Fu J, Buss SN, Jossinet F, Jobe A, et al. High-resolution cryo-electron microscopy structure of the trypanosoma brucei ribosome. *Nature* 2013;**494**:385–9.
25. Verschoor A, Srivastava S, Grassucci R, Frank J. Native 3D structure of eukaryotic 80S ribosome: morphological homology with the *E. coli* 70S ribosome. *J Cell Biol* 1996;**133**:495–505.
26. Chothia C, Lesk AM. The relation between the divergence of sequence and structure in proteins. *EMBO J* 1986;**5**:823–6.
27. Venclovas C, Margelevičius M. Comparative modeling in CASP6 using consensus approach to template selection, sequence–structure alignment, and structure assessment. *Proteins* 2005;**61 Suppl 7**:S99–105.
28. Guex N, Peitsch MC. Swiss-model and the swiss-pdb viewer: an environment for comparative protein modeling. *Electrophoresis* 1997;**18**:2714–23.

29. Lund O, Frimand K, Gorodkin J, Bohr H, Bohr J, Hansen J, et al. Protein distance constraints predicted by neural networks and probability density functions. *Protein Eng* 1997;**10**:1241–8.
30. Sutcliffe MJ, Haneef I, Carney D, Blundell TL. Knowledge based modelling of homologous proteins, part I: three-dimensional frameworks derived from the simultaneous superposition of multiple structures. *Protein Eng* 1987;**1**:377–84.
31. Scott WR, Hünenberger PH, Tironi IG, Mark AE, Billeter SR, Fennen J, et al. The GROMOS biomolecular simulation program package. *J Phys Chem* 1999;**103**:3596–607.
32. Chen VB, Arendall III WB, Headd JJ, Keedy DA, Immormino RM, Kapral GJ, et al. MolProbity: all-atom structure validation for macromolecular crystallography. *Acta Crystallogr D Biol Crystallogr* 2010;**66**:12–21.
33. Laskowski RA, Rullmann JA, MacArthur MW, Kaptein R, Thornton JM. Aqua and PROCHECK-NMR: programs for checking the quality of protein structures solved by nmr. *J Biomol NMR* 1996;**8**:477–86.
34. Alkemar G, Nygård O. Secondary structure of two regions in expansion segments ES3 and ES6 with the potential of forming a tertiary interaction in eukaryotic 40S ribosomal subunits. *RNA* 2004;**10**:403–11.
35. Chandramouli P, Topf M, Ménétret JF, Eswar N, Cannone JJ, Gutell RR, et al. Structure of the mammalian 80S ribosome at 8.7 Å resolution. *Structure* 2008;**16**:535–48.
36. Klinge S, Voigts-Hoffmann F, Leibundgut M, Ban N. Atomic structures of the eukaryotic ribosome. *Trends Biochem Sci* 2012;**37**:189–98.
37. Omotajo D, Tate T, Cho H, Choudhary M. Distribution and diversity of ribosome binding sites in prokaryotic genomes. *BMC Genom* 2015;**16**:604.
38. Kuroda H, Sugiura M. Processing of the 5′-UTR and existence of protein factors that regulate translation of tobacco chloroplast psbN mRNA. *Plant Mol Biol* 2014;**86**:585–93.
39. Lo Conte L, Brenner SE, Hubbard TJ, Chothia C, Murzin AG. SCOP database in 2002: refinements accommodate structural genomics. *Nucleic Acids Res* 2002;**30**:264–7.
40. Andreeva A, Howorth D, Chandonia JM, Brenner SE, Hubbard TJ, Chothia C, et al. Data growth and its impact on the scop database: new developments. *Nucleic Acids Res* 2008;**36 Suppl 1**:D419–25.
41. Douthwaite JA, Groves MA, Dufner P, Jermutus L. An improved method for an efficient and easily accessible eukaryotic ribosome display technology. *Protein Eng Des Sel* 2006;**19**:85–90.
42. Han J, Kim M, Oum JH, Myung H, Lee SW, Jeong S, et al. RACK-1, a receptor for activated C kinase, interacts with the transcription factor NFAT and represses its transactivation. *Mol Cells* 2002;**14**:420–4.
43. Ramakrishnan V. Molecular biology. The eukaryotic ribosome. *Science* 2011;**331**:681–2.
44. Schmeing TM, Ramakrishnan V. What recent ribosome structures have revealed about the mechanism of translation. *Nature* 2009;**461**:1234–42.